Phys Chem Minerals (1994) 21:191–206

PHYSICS AND CHEMISTRY OF MINERALS

High-resolution Parallel Electron Energy-loss Spectroscopy of Mn $L_{2,3}$-Edges in Inorganic Manganese Compounds

L.A.J. Garvie*, A.J. Craven

Department of Physics and Astronomy, University of Glasgow, Glasgow G12 8QQ, UK, Fax 3349029

Received November 8, 1993 / Revised, accepted January 14, 1994

Abstract. Parallel electron energy-loss spectroscopy (PEELS) in a scanning transmission electron microscope (STEM) was used to record the Mn $L_{2,3}$-edges from a range of natural and synthetic manganese containing materials, covering valences 0, II, III, IV and VII, with an energy resolution of ca. 0.5 eV. The Mn $L_{2,3}$ electron-loss near-edge structure (ELNES) of these edges provided a sensitive fingerprint of its valence. The Mn^{2+} $L_{2,3}$-edges show little sensitivity to the local site symmetry of the ligands surrounding the manganese. This is illustrated by comparing the Mn $L_{2,3}$-edges from 4-, 6- and 8-fold coordinated Mn^{2+}. In contrast, the Mn L_3-edges from Mn^{3+} and Mn^{4+} containing minerals exhibited ELNES that are interpreted in terms of a crystal-field splitting of the 3d electrons, governed by the symmetry of the surrounding ligands. The Mn L_3-edges for octahedrally coordinated Mn^{2+}, Mn^{3+} and Mn^{4+} showed variations in their ELNES that were sensitive to the crystal-field strength. The crystal-field strength (10Dq) was measured from these edges and compared very well with published optically determined values. The magnitude of 10Dq measured from the Mn L_3-edges and their O K-edge prepeaks of the manganese oxides were almost identical. This further confirms that the value of 10Dq measured at the Mn L_3-edge is correct. Selected spectra are compared with theoretical 2p atomic multiplet spectra and the differences and similarities are explained in terms of the covalency and site symmetry of the manganese. The Mn L_3-edges allow the valence of the manganese to be ascertained, even in multivalent state materials, and can also be used to determine 10Dq.

Introduction

Electron energy-loss spectroscopy (EELS) in a transmission electron microscope has been widely used to determine the oxidation state (Leapman et al. 1982; Otten and Buseck 1987; Krishnan 1990; Brydson et al. 1992; Garvie and Craven 1993, 1994a, 1994b) and coordination/site symmetry (de Groot et al. 1992; Garvie and Craven 1993; Brydson et al. 1993) of the 3d transition metals (TM) from their $L_{2,3}$-edges. X-ray absorption spectroscopy (XAS) and EELS studies of the 3d transition metal containing materials have shown that their $L_{2,3}$-edges can also reflect the spin state of the metal (van der Laan et al. 1988; Kurata et al. 1990; Cramer et al. 1991; de Groot et al. 1993). Several studies have concentrated on Mn-containing materials (Rask et al. 1987; Paterson and Krivanek 1990; Krivanek and Paterson 1990; Kurata and Colliex 1993; Garvie and Craven 1993) using peak heights, chemical shift or the electron-loss near-edge structure (ELNES) of the manganese $L_{2,3}$-edges to determine the oxidation state. Manganese belongs to the 3d TM series and the ground state of the isolated atom has the electron configuration $[Ar]4s^23d^5$. Its chemistry is characterised by its partially filled d-shells in contrast to the main group elements where bonding is dominated by s and p orbitals. In these compounds not only is there strong interaction between the cation and anion sp orbitals but also interaction between the metal d- and anion p-orbitals. The 3d-electrons in the 3d TM form part of the outer electron structure and as such they are strongly influenced by their surroundings. Since the Mn $L_{2,3}$ ELNES is dominated by dipole allowed transitions to states of 3d character, it is expected that the $L_{2,3}$-edge will be modified by the environment of the 3d electrons such as the symmetry and type of ligands surrounding the cation. In order to be able to interpret the crystal chemical environment from the fine multiplet structure of the $L_{2,3}$-edges it is essential to use high energy resolution when collecting the $L_{2,3}$-edge data. This is a result of the small lifetime broadening of the 3d TM 2p levels which ranges from 0.2 eV for Ti to 0.4 eV for Ni (Fink et al. 1985; Abbate et al. 1991).

Manganese can form compounds with a large number of oxidation states ranging from Mn^{3-} in $Mn(NO)_3CO$

* *Present address:* Department of Geology, Arizona State University, Tempe, Arizona 85287-1404, USA

Correspondence to: L.A.J. Garvie

through Mn^0 to Mn^{7+} in $KMnO_4$ (Cotton and Wilkinson 1988). Although manganese can reside with coordination numbers between 2 and 8, it is typically octahedrally bonded for oxidation states between II and IV. Higher oxidation states of manganese are more usually tetrahedrally coordinated. In nature, manganese occurs in minerals in the three oxidation states Mn^{2+}, Mn^{3+} and Mn^{4+} and minerals with multivalent Mn cations are quite common. The electronic configuration of Mn^{2+}, $3d^5$, and Mn^{3+}, $3d^4$, implies that they may exist in either the high-spin or low-spin state. Minerals containing $^{[6]}Mn^{2+}$ in the low-spin state are unlikely to occur in nature as only strong field-ligands, such as CN^-, can overcome the large exchange splitting of the Mn^{2+} crystal-field orbitals (Sherman 1984). The same is not true for $^{[6]}Mn^{3+}$ which theoretically could exist in the low-spin spin state while bonded to the normal mineral forming ligands such as O^{2-} and OH^-, but is stabilised in the high-spin state via distortion of the coordination environment due to the Jahn-Teller effect. Octahedrally coordinated Mn^{4+} has three 3d electrons and so can only exist in the high-spin state. Mn^{2+} occurs in a range of different coordinations such as tetrahedral, five-fold and eight-fold coordinations. Mn^{3+} most commonly resides in an octahedral environment and in minerals Mn^{4+} cations occur only in octahedrally coordinated sites.

Metal $L_{2,3}$ ELNES have been modelled using several techniques such as multiconfiguration Dirac-Fock (Waddington et al. 1986) and systematic linear augmented plane-wave (Mattheiss and Dietz 1980) methods. The TM $L_{2,3}$-edges cannot be modelled successfully in terms of a one-particle density of states because of the large degree of electron correlation between the 3d electrons in the partially filled 3d-shells. The most successful method is the ligand-field multiplet approach (LFM) (Yamaguchi et al. 1982; Thole et al. 1985; van der Laan et al. 1986; de Groot et al. 1990a, 1990b; van der Laan and Kirkman 1992; de Groot et al. 1993) which explicitly takes into account the d–d electron interactions. Molecular orbital (MO) calculations have also been applied to an MnO_6^{n-} cluster. Sherman (1984) used a spin unrestricted self-consistent field SCF Xα method to calculate the MOs for octahedrally coordinated Mn^{2+}, Mn^{3+} and Mn^{4+} in O_h (octahedral) symmetry.

This study is an extension of previous EELS work done on Mn-containing compounds by examining a larger set of inorganic Mn-containing materials and illustrates the Mn $L_{2,3}$-edges for different valences, coordinations and site symmetries as well as for mixed valent materials.

Materials and Methods

Twenty-five manganese containing materials were studied covering oxidation states 0, II, III, IV and VII. They are listed in Table 1 which gives details of the oxidation state, the coordination number of the manganese and the structure type of the compounds. The materials chosen were on the whole electron-beam stable and they allowed data to be collected that were free from electron-beam induced effects. The majority of the samples were natural minerals except for $MnFe_2O_4$, $SrMnO_3$, $KMnO_4$, and Mn. All of the samples were prepared by crushing selected grains of materials in acetone and drying a drop on a lacy carbon film. Potassium permanganate was dissolved in acetone and recrystallized as thin plates on the lacy carbon film. EELS data were recorded from thin, electron-beam transparent areas over holes in the support film. Manganese metal was further prepared in the electron microscope by intense electron-beam irradiation of a metal grain (ca. 3 μm diameter) supported on the holey carbon film. This caused the metal to melt and thin fingers of pure Mn metal, free from the O detected in the initial grain, grew from the side of the large grain.

The EELS data were obtained using a Gatan model 666 parallel EELS spectrometer mounted on a VG HB5 STEM. The HB5 has a cold field-emission gun (FEG) and was operated at an accelerating voltage of 100 kV with a probe semi-angle of 11 mrad and a collection angle of 12.5 mrad. The emission current drawn from the FEG was ca. 5 nA which resulted in an energy resolution of ca. 0.35 eV at the zero loss peak (ZLP). The resolution at the Mn L_3-edge was better than 0.5 eV as indicated by the features resolved at the Mn L_3-edge from bixbyite.

The dispersion of the spectrometer system and the energies of the features present on the edges were determined by applying known voltages to the electrostatically isolated drift tube within which the electrons traverse the spectrometer magnet (Krivanek et al. 1987). The Ni L_3-edge in NiO, which has been determined to be at 853.2 eV by X-ray absorption spectroscopy (van der Laan et al. 1986), was used to calibrate the system. There can be day to day variations of ± 0.5 eV in the absolute value of the energy of a peak measured on the spectrometer. The position of two edges can be compared to within ± 0.2 eV by recording the edges from different materials on the same microscope grid on the same day. Relative peak positions on the same edge can be determined with an accuracy of ± 0.01 eV. Energy dispersions of 0.1 eV or 0.05 eV were used allowing the fine structure of the Mn $L_{2,3}$-edges to be clearly discerned. The spectra were collected with integration times in the range 4 to 16 seconds using a 1 nm diameter probe scanned over a raster measuring typically 60 nm × 50 nm at TV rate. For materials that showed evidence of electron beam damage, the probe was defocused to ca. 100 nm. In general the beam sensitivity of the materials ranged from very low for the Mn^{2+} compounds through moderate for the Mn^{4+} oxides to extremely beam sensitive for $KMnO_4$. Collection of the Mn $L_{2,3}$-edges from $KMnO_4$ required special acquisition procedures, i.e. highly defocused beam, short integration time (<2 s), low beam current and moving over the sample during acquisition thus continuously exposing new material to the electron beam. After the core-loss data were collected the dark currents appropriate to the acquisition conditions were recorded and subtracted from the spectra. The effects of multiple scattering in the specimen and tailing due to light spreading in the detector were

Table 1. Simplified formula, mineral name (where appropriate), valence and coordination of the manganese, structure type and reference for the Mn-containing materials studied

Chemical formula	Mineral name	Mn valency	CN[a]	Structure type	Ref.
Mn[b,c]	manganese	0	–	–	–
MnO	manganosite	2+	6	rock salt	1
$MnCO_3$	rhodochrosite	2+	6	calcite	1
MnF_2[b]	–	2+	6	distorted rutile	2
$MnSiO_3$	rhodonite	2+	6,7	pyroxenoid	1
$Li(Mn,Ca)PO_4$	lithiophilite	2+	6	olivine-like	3
$MnFe_2O_4$[b]	jacobsite	2+	4	spinel	4
$Mn_3Al_2(SiO_4)_3$	spessartine	2+	8	garnet	1
MnS_2	hauerite	2+	6	pyrite	5
α-MnS	alabandite	2+	6	rock salt	5
$Mn_3(B_3B_4O_{12})OCl$	chambersite	2+	5	boracite[d]	6
$Mn_4(BeSiO_4)_3S$	helvite	2+	4	sodalite-like	7
γ-MnOOH	manganite	3+	6	distorted rutile	8
$KLiMn_2Si_4O_{12}$	norrishite	3+	6	mica	9
$Ca_4Mn_3O_3(BO_3)_3(CO_3)$	gaudefroyite	3+	6	gaudefroyite	10
$(Mn,Fe)_2O_3$	bixbyite	3+	6	fluorite	8
MnO_2	ramsdellite	4+	6	diaspore	11
β-MnO_2	pyrolusite	4+	6	tetragonal rutile	8
$ZnMn_3O_7 \cdot 3H_2O$	chalcophanite	4+	6	phyllomanganate	8
$(MnO_2)_{2-x}(OH)_x(Co,Ni)_{1-y}(OH)_{2-2y+x} \cdot nH_2O$	asbolan	4+	6	phyllomanganate	12
$(Na,Ca,K)(Mn,Mg)_6O_{12} \cdot nH_2O$	todorokite	4+	6	3 × 3 tunnel	8
$SrMnO_3$[b]	–	4+	6	see reference	13
$Mn^{2+}Mn^{3+}{}_6SiO_{12}$	braunite	2+,3+	8,6	bixbyite-like	14
α-$Mn^{2+}Mn^{3+}{}_2O_4$	hausmannite	2+,3+	4,6	distorted-spinel	15
$KMnO_4$	–	7+	4	manganate	16

[a] CN-coordination number
[b] synthetic
[c] the exact form is unknown due to the preparation procedure (see text)
[d] this reference is for the Mg-analogue as no detailed crystallographic data exist for chambersite

1. Smyth and Bish (1988)
2. Stout (1959)
3. Geller and Durand (1960)
4. Allan et al. (1988)
5. Furuseth and Kjekshus (1965)
6. Dowty and Clark (1973)
7. Holloway et al. (1972)
8. Waychunas (1991)
9. Tyrna and Guggenheim (1991)
10. Yakubovich et al. (1975)
11. Miura et al. (1990)
12. Manceau et al. (1987)
13. Battle et al. (1988)
14. Moore and Araki (1976)
15. Kaczmarek and Wolska (1993)
16. Palenik (1967)

then removed by Fourier-ratio deconvolution using the low-loss spectrum (Egerton 1986).

$L_{2,3}$-Edge Shapes

In an isolated Mn atom, the allowed transitions close to the threshold of the $L_{2,3}$-edge are from core Mn 2p electrons to 3d and 4s states, i.e. dipole allowed transitions with a small scattering vector. Transitions to the 3d level dominate in the $L_{2,3}$ white lines, so contributions from 2p → 4s will be negligible in the overall $L_{2,3}$ absorption/ionisation edges (de Groot et al. 1990a, 1990b; van der Laan and Kirkman 1992) as they are much weaker and add to the background at higher energies beyond the $L_{2,3}$ ELNES. The 2p to 3d transitions in Mn give rise to two edges, separated by ca. 10 eV, due to the spin-orbit splitting of the 2p core level arising from the $2p_{3/2}$ (L_3-edge) and $2p_{1/2}$ (L_2-edge) levels. Owing to the large number of unoccupied states in the narrow 3d band, each edge has sharp peaks or white lines at the threshold. The width of the L_2 peak is broader than the L_3 peak due to the Coster-Kronig Auger decay channel available to the $2p_{1/2}$ core hole state but not to the $2p_{3/2}$ state. This reduces the lifetime of the $2p_{1/2}$ core hole and results in a relative broadening of its energy.

The $L_{2,3}$-edge spectra can be thought of as resulting from quasiatomic transitions from the $2p^63d^n$ initial state to the $2p^53d^{n+1}$ final state. The quasiatomic nature of the $L_{2,3}$-edge is caused by the strong coupling between the 3d electrons and the 2p core hole and hence the $L_{2,3}$ white lines arise from transitions to bound atomic-like states. Interaction between the $3d^n$ electrons in the $2p^63d^n$ state gives rise to an initial state multiplet. In the $2p^53d^{n+1}$ final state a large number of possible dipole-allowed states are caused by the 2p core hole spin-orbit coupling and the interaction of the core hole with the distribution of the electrons in the final state. An atomic multiplet spectrum then arises due to the energies

and intensities of the dipole-allowed transitions between the initial state multiplet and all final states. The resulting spectrum will be broadened due to lifetime effects as well as vibration and hybridisation in the final state. One of the most important effects to modify the spectrum is the influence of the crystal-field due to the ligands surrounding the atom. This reduces the symmetry of the degenerate d orbitals from spherical symmetry (O_3) to that governed by the symmetry of the ligands surrounding the cation and further splits the initial and final state multiplets. Assuming that the crystal-field does not change the ground state from the atomic situation, which is true for dominantly ionic high-spin manganese compounds, the effect of the ligands on the spectrum will be to split and/or shift energy levels and modify the transition matrix elements. This causes a change in the spectrum shape which may include new final states that were forbidden in spherical symmetry. As illustrated by the theoretical atomic multiplet spectra for 3d transition elements (de Groot et al. 1990a, 1990b; van der Laan and Kirkman 1992) the magnitude of the crystal-field affects both the relative intensities and energy positions of the observed transitions. In an octahedral field with O_h symmetry the electrostatic interaction of the Mn 3d orbitals with the surrounding anions causes the degenerate 3d-orbitals to split into orbitals with t_{2g} (triply degenerate) and e_g (doubly degenerate) character. These orbitals can be split further depending on the nature and distribution of the anions around the transition metal. The two sets of orbitals, t_{2g} and e_g, are separated by an energy 10Dq which is a measure of the crystal-field strength. The e_g orbitals are directed towards the anions raising their energies whereas the t_{2g} orbitals are rather delocalized over the three metal ligand planes and thus their energies are reduced. Figure 1 illustrates the effect of several common ligand symmetries upon the energy arrangement of the transition metal 3d-orbitals. The magnitude of the crystal-field splitting depends on the oxidation state, coordination and site symmetry of the

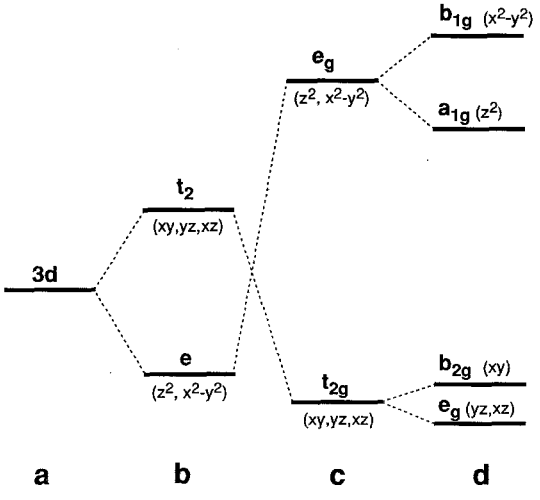

Fig. 1. Examples of crystal-field splittings of the 3d transition metal d electrons in: **a** spherically perturbed d shell, O_3 symmetry; **b** tetrahedral, T_d; **c** octahedral, O_h; and **d** weak field tetragonal, D_{4h}

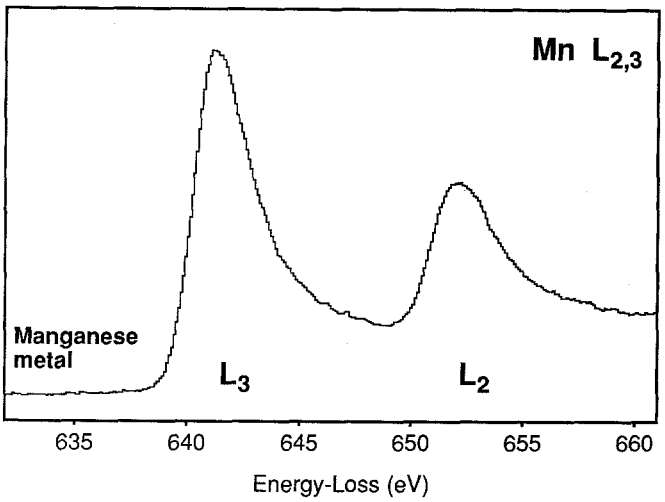

Fig. 2. Mn $L_{2,3}$-edge from manganese metal. The position of the separate L_3- and L_2-edges are indicated

transition metal and on the nature of the coordinating anions. Another way of describing the electron energies is by MO theory. From a MO point of view, the t_{2g} and e_g orbitals are actually the corresponding $2t^*_{2g}$ and $3e^*_g$ antibonding orbitals of the bonding $1t_{2g}$ and $2e_g$ valence band MOs (Sherman 1984).

Manganese 0

Metallic manganese has the ground state electron configuration $[Ar]4s^23d^5$ and term $^6S_{5/2}$. Figure 2 illustrates the $L_{2,3}$-edge for manganese metal and shows two broad asymmetrical peaks at 641.3 and 652 eV. Both edges exhibit broadening towards the high-energy side. The larger widths of final states in the metal compared to those in an insulator results in broad L_3- and L_2-edges without any resolvable multiplet structure. Similar high resolution EELS spectra of manganese metal, with an energy resolution of 0.6 eV, failed to resolve any multiplet splitting of the Mn $L_{2,3}$ edge (Fink 1985; Fink et al. 1985; Thole et al. 1985). In metals, the 2p core hole is screened by valence electrons so there is less interaction between the core hole and 3d electrons. Hence the spectrum reflects more of the character of the d density of states unlike the $L_{2,3}$-edge spectra from the 3d TM compounds where the quasiatomic picture is more predominant (Brydson 1991).

Manganese II

The high-spin ground state term for Mn^{2+} in an octahedral environment is $^6A_{1g}$ $[(t^+{}_{2g})^3(e^+{}_g)^2]$. There are a total of five unpaired electrons occupying the t_{2g} and e_g orbitals. For $^{[4]}Mn^{2+}$ with perfect T_d symmetry, the crystal-field splitting of the d-orbitals is the reverse of that in O_h symmetry (Fig. 1 b) and the ion has the ground state $^6A_1[(e^+)^2(t^+{}_2)^3]$. The subscript g is dropped in T_d symmetry since we no longer have inversion symmetry.

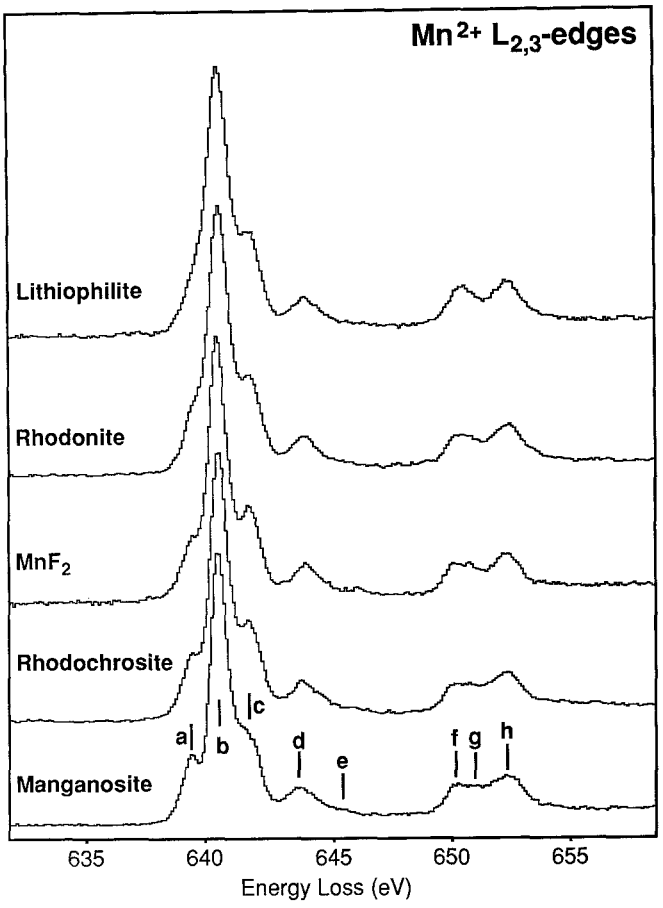

Fig. 3. Mn $L_{2,3}$-edges from the octahedrally coordinated Mn^{2+} materials, manganosite, rhodochrosite, MnF_2, rhodonite and lithiophilite. The *vertical bars* above the manganosite spectrum indicate the positions of the individual peak maxima. The spectra have been aligned with respect to peak (b) on the L_3-edge and ordered from manganosite to lithiophorite with respect to decrease in the separation between peaks (a) and (b)

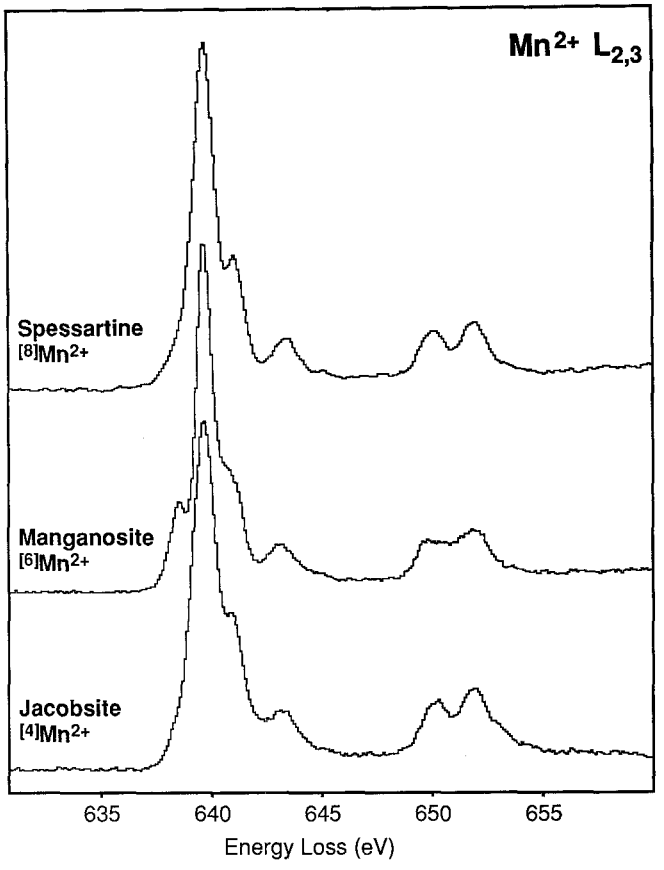

Fig. 4. Comparison of the Mn $L_{2,3}$-edges from tetrahedrally (jacobsite), octahedrally (manganosite) and dodecahedrally (spessartine) coordinated Mn^{2+}

Assuming the same metal to ligand distances in O_h and T_d symmetry, the magnitude of the 10Dq in tetrahedral symmetry is $^4/_9$ of that in octahedral symmetry. With the anions arranged in a square with the Mn at the centre (D_2 site symmetry) the magnitude of the crystal-field splitting is $^8/_9$ that in O_h symmetry (Manning 1967). All of the compounds studied in this work contain manganese in the high-spin state. Although not studied in this work, low-spin manganese compounds have the $^2T_2[(t^+{}_{2g})^3(t^-{}_{2g})^2]$ ground state and thus have a significantly different $L_{2,3}$-edge shape (Cramer et al. 1991).

The $L_{2,3}$-edge shapes obtained from the Mn^{2+} minerals in Table 1 are shown in Figs. 3, 4, and 5. Figure 3 presents edges from $^{[6]}Mn^{2+}$ coordinated by dominantly ionic ligands. Fig. 4 compares Mn^{2+} $L_{2,3}$-edges in 4-, 6- and 8-fold coordination and Fig. 5 shows the effects of covalency, unusual coordination, and mixed ligand bonding. The edge shapes are all similar but there are considerable variations in the visibility of the fine details. The separate peaks are labelled for manganosite in Fig. 3. All the edges show peaks (b), (c), (d), (f) and (h). Minerals with 6-fold coordination usually show evidence of peak (a) which is especially prominent for manganosite, rhodochrosite and MnF_2. Peaks (e) and (g) are always weak and cannot be discerned in the majority of the spectra. The absolute energy values of the most intense peak (b) lie in the range 639.5 eV to 640.6 eV for all of the Mn^{2+} compounds studied here. Manganosite was studied on several occasions and gave an absolute L_3-edge energy value of 640.3 ± 0.5 eV.

In general it is expected that the fine detail present on the edges would be influenced by the nature of the ligands, their number and their arrangement. The $L_{2,3}$-edge shapes shown in Fig. 3 are from minerals in which the Mn^{2+} is surrounded by 6 ligands where the bonding is, to a good approximation, ionic. They are ordered from manganosite to lithiophilite in terms of the decreasing energy between the pre-peak (a) and the most intense peak (b) on the L_3-edge. This also corresponds to a decrease in intensity of the weak peak (g) on the L_2-edge. The differences in the $L_{2,3}$-edges may be explained in terms of the crystal-field strength from the ligands and distortions from O_h symmetry. Manganese in manganosite has O_h site symmetry with six equidistant oxygen ligands (Smyth and Bish 1988). In rhodochrosite and MnF_2 the Mn sits in a slightly distorted octahedral site with trigonal and tetragonal distortions respectively. These deviations from O_h symmetry do not appear to have caused further splitting of the $L_{2,3}$-edges. This is in accordance with the results of van der Laan and Kirkman (1992) who state that symmetries lower than O_h,

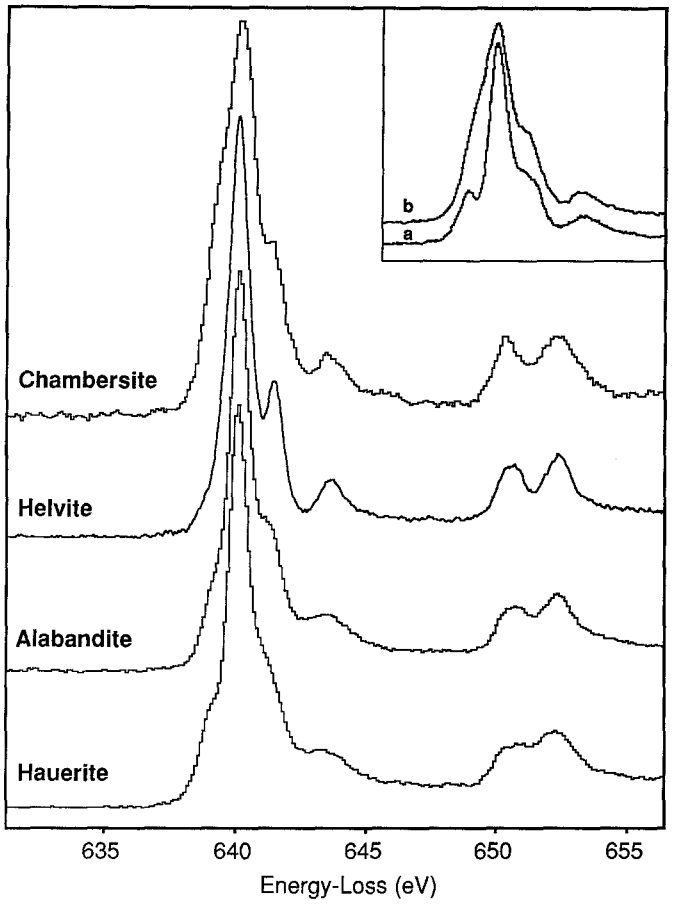

Fig. 5. Mn $L_{2,3}$-edges from the four minerals hauerite, alabandite, helvite and chambersite. The *inset* compares the L_3-edge from (a) manganosite and (b) chambersite

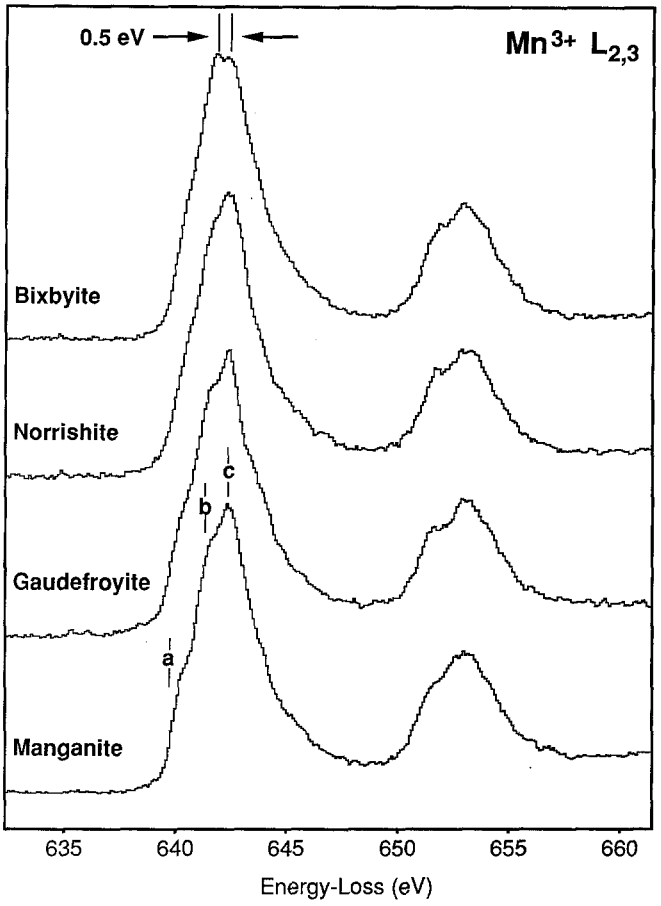

Fig. 6. Mn $L_{2,3}$-edges from the Mn^{3+} containing minerals manganite, gaudefroyite, norrishite and bixbyite. The *vertical bars* on the L_3-edge of manganite indicate the positions of partially resolved peaks. The L_3-edge for bixbyite is split into two peaks separated by ca. 0.5 eV

where the non-cubic distortion is small, will give similar spectra to those with O_h symmetry. Thus, as expected, the Mn $L_{2,3}$-edges from rhodochrosite and MnF_2 are similar in shape to the Mn $L_{2,3}$-edge from manganosite. Rhodonite contains five distinct Mn sites one of which is 7-fold coordinated (Smyth and Bish 1988) and all have point symmetry C_1 with large bond and angular variations. Lithiophillite has an orthorhombic olivine-like structure (Geller and Durand 1960) with highly distorted Mn octahedra (point symmetry C_s). It is apparent from the $L_{2,3}$-edges from rhodonite and lithiophilite that Mn octahedra with very low symmetry still do not have a large effect on the edge shape even though the non-cubic distortions are large.

The Mn $L_{2,3}$-edges from synthetic jacobsite ($^{[4]}Mn^{2+}$) and spessartine ($^{[8]}Mn^{2+}$) are very similar to $^{[6]}Mn^{2+}$ with O_h symmetry (Fig. 4). Using optical spectroscopy, Manning (1967) did not observe any additional splittings of the Mn^{2+} bands due to its D_2 site symmetry in spessartine. The atomic multiplet calculations for $^{[4]}Mn^{2+}$ with T_d symmetry and $^{[6]}Mn^{2+}$ with O_h symmetry are very similar (van der Laan and Kirkman 1992) and thus would explain the close similarity between the Mn $L_{2,3}$-edges for jacobsite and manganosite.

Two other effects can change the shape of Mn $L_{2,3}$-edges: a) an increase in covalent character between the transition metal and its anions, and b) the bonding of the manganese to more than one type of ligand. Hauerite and alabandite exhibit similar Mn $L_{2,3}$-edge shapes to the Mn $L_{2,3}$-edges from manganosite but the L_3-edge shows poor resolution of the multiplet features after the main L_3 peak, peaks (c) and (d). These differences may be due to the significant amount of covalent bonding between the manganese and sulphur. Similar changes were also observed in covalent Ni^{2+} compounds (van der Laan et al. 1986) and attributed to an increase in covalent mixing in final states which reduces the multiplet structure with the appearance of screening satellites. In helvite, the Mn^{2+} cation is on a triad axis and sits in a fairly regular tetrahedral site coordinated to three oxygen atoms and one sulphur atom. The Mn $L_{2,3}$-edge for helvite does not show any significant differences in the ELNES that could be related to the bonding of the Mn to two different ligands. The crystal structure of chambersite is more complex than the other minerals studied so far. At room temperature it contains three distinct metal sites (Belov et al. 1975) that are located in hybrid square pyramidal/trigonal pyramidal five coor-

Table 2. Comparison of optical and EELS 10Dq measurements from selected Mn^{2+} compounds. Error in EELS values is ± 0.02 eV

Material	Optical (eV)	Ref.	EELS (eV)
manganosite	1.21	1	1.13
rhodochrosite	0.93	2	1.12
MnF_2	0.97	3	1.01
rhodonite	1.02	2	0.99
hauerite[a]	–	–	0.90
alabandite	0.88	4	0.77
spessartine[b]	0.87	5	–
lithiophilite[b]	0.84	2	–

[a] corresponding optical data unknown
[b] t_{2g} peak very weak or not present
1. Pratt and Coelho (1959)
2. Keester and White (1968)
3. Stout (1959)
4. Duffy (1990)
5. Manning (1967)

dinated sites (Dowdy and Clark 1973). Each metal atom is bonded to a distorted rectangular base of oxygen atoms, and a chlorine atom which serves as the apex to the pyramid. The $L_{2,3}$-edge from chambersite retains the same basic shape as the other Mn^{2+} $L_{2,3}$-edges although the L_3-edge is appreciably broadened and shows evidence of at least two partially resolved peaks on the low-energy side of the L_3-edge. This is illustrated in the inset of Fig. 5 which compares the L_3-edge from chambersite with manganosite. Minerals containing five-fold coordinated Mn^{2+} are unusual and it is uncertain whether the differences in the $L_{2,3}$-edges between manganosite and chambersite are due to the five-fold site symmetry, the mixture of different ligand types or a combination of both in chambersite.

The energy splitting between peaks (a) and (b) in selected spectra in Figs. 3 and 5 were determined by fitting Gaussians to the two peaks and measuring the energy difference between them. Table 2 compares the 10Dq values determined by optical spectroscopy with these measurements for a number of the Mn^{2+} compounds and shows the good agreement between the two sets of data. The close correspondence between the optically determined 10Dq values and those determined from the L_3-edge may allow us to assign the pre-peak (a) to transitions to orbitals with t_{2g} character and peak (b) to transitions to orbitals with e_g character. An approximate value of 10Dq for jacobsite can be estimated by comparing its $^{[4]}Mn^{2+}$ L_3-edge with those calculated for Mn^{2+} with T_d symmetry in van der Laan and Kirkman (1992). A crystal-field strength of 0.5 eV gives the best match. Taking the measured value of 10Dq in $^{[6]}Mn^{2+}$ with O_h symmetry as 1.13 eV measured from manganosite, the value for T_d symmetry is ca. 0.50 eV in good agreement with the above value and close to the optically determined value of 0.41 eV from $MnCl_4^{2-}$ (Lever 1984).

Use of the L_3 multiplet structure to directly measure 10Dq must be treated with caution since the theoretical multiplet spectra illustrate that the $L_{2,3}$-edges consist of a large number of possible final states. It is therefore difficult to assign a simple ligand-field splitting to these edges and in general the energy splitting on the L_3-edges is not equal to the energy value of 10Dq used in the calculation (de Groot et al. 1990a). Another method to determine 10Dq is to compare the $L_{2,3}$-edges directly with calculated atomic multiplet spectra and to alter the parameters to give the best fit to the experimental data. Cramer et al. (1991) found that the 10Dq values determined in this way by XAS data from a number of Mn compounds are approximately 25% smaller than those determined by UV-visible spectroscopy. However, it is possible that these differences are a result of compensation of approximations in the calculations by an error in the 10Dq value used.

Manganese III

High-spin Mn^{3+} has four 3d electrons and exists in the ^5E_g $[(t^+{}_{2g})^3(e^+{}_g)^1]$ ground state in an octahedral environment. For Mn^{3+}, the octahedral complexes are subject to strong Jahn-Teller distortion. This results from the odd number of e_g electrons which cause elongation of two trans bonds with little difference in the lengths of the other four Mn–O distances and results in a reduction of the symmetry from O_h to D_{4h}. Although the Jahn-Teller theorem predicts that the octahedron may be either elongated or compressed, experimental evidence shows that octahedra are predominantly elongated (Lever 1984). Thus the t_{2g} and e_g orbitals, arising from a crystal-field of O_h symmetry, are further split. The triply degenerate t_{2g} orbital splits into an e_g degenerate pair (d_{xz} and d_{yz}) and a b_{2g} orbital (d_{xy}) and the e_g orbital splits into an a_{1g} (d_{z^2}) and b_{1g} ($d_{x^2-y^2}$) orbital (Fig. 1d). In D_{4h} symmetry with a weak tetragonal distortion, high-spin d^4 Mn has the following ground state term and orbital assignments ^5B_g $[(e^+{}_g)^2(b^+{}_{2g})^1(a^+{}_{1g})^1(b^+{}_{1g})^1]$. The crystal-field splitting in D_{4h} symmetry is defined as the energy difference between the b_{1g} and b_{2g} orbitals (Sherman 1984; Lever 1984). This was calculated to be 2.42 eV using the SCF Xα calculations of Sherman (1984) for the MnO_6^{n-} cluster. Optically determined values of 10Dq for Mn^{3+} range from 2.18 eV in Na_3MnF_6 (Köhler et al. 1978) through 2.25 eV in epidote to 2.75 eV in andalusite (Lever 1984).

The experimental EELS spectra for the Mn^{3+} $L_{2,3}$-edges all have very similar shapes (Fig. 6) without any clearly resolved multiplet splitting. Unlike the Mn^{2+} compounds there is no well resolved multiplet structure after the L_3 peak maximum. For manganite, gaudefroyite and norrishite the L_3 peak maximum is at ca. 642 eV. These minerals exhibit two partially resolved peaks (labelled (a) and (b) in Fig. 6) which are ca. 2.3 and 1 eV from peak (c). These minerals all contain a single $^{[6]}Mn^{3+}$ site in a Jahn-Teller distorted environment. Manganite illustrates the Jahn-Teller effect very well since the octahedra are stretched with four close (1.868, 1.878, 1.965, 1.981 Å) and two distant (2.199, 2.333 Å) oxygen ligands (Waychunas 1991). The Mn L_3-edge for bixbyite differs in shape from the other Mn^{3+} compounds studied in that the peak maximum is actually resolved into two peaks separated by ca. 0.5 eV. This

peak splitting was observed in most of the L_3-edges from bixbyite and so is unlikely to be due to noise in the spectrum. The differences between the bixbyite Mn L_3-edge and the other studied Mn^{3+} minerals may be due to different Mn site symmetries. In bixbyite there are two inequivalent $^{[6]}Mn^{3+}$ sites (Geller 1971; Smyth and Bish 1988). The first one has six very similar Mn–O distances (C_{3i} site symmetry) and the second one is highly distorted (C_2 site symmetry) with three different sets of Mn–O distances.

In all of the L_3-edges in Fig. 6 the approximate energy difference between the first partially resolved edge and the peak maximum is ca. 2.3 eV which is between the 10Dq determined for Mn^{3+} in epidote and andalusite (Lever 1984). To better determine the energies of the partially resolved peaks in the Mn^{3+} L_3-edges, Gaussian peaks were fitted to the Mn L_3-edge from manganite. Fig. 7 shows the positions of three Gaussian peaks used to simulate the L_3-edge and a possible MO assignment of the features on the Mn L_3-edge based on D_{4h} symmetry splitting of the d orbitals. The positions and widths of the Gaussian peaks used to model the Mn^{3+} L_3-edge were chosen so as to give the optimum fit to the experimental edge. This gives the following energy separations, $(t_{2g})-b_{1g}=2.28$ eV and $a_{1g}-b_{1g}=1.15$ eV. In D_{4h} symmetry crystal-field theory predicts that the Jahn-Teller splitting of the t_{2g} orbitals will be smaller than the splitting of the e_g orbital. The t_{2g} is not resolved into two peaks representing the b_{2g} and e_g orbitals as they are typically separated by only ca. 0.2 eV (Köhler et al. 1978). The energy separations between the three orbitals are very close to the values determined by optical spectroscopy for a large number of tetragonal Mn fluorides (Oelkrug 1971; Allen and Warren 1971; Köhler et al. 1978). Electron configurations are represented by lower case letters and upper case letters represent the total wavefunction described as a group theoretical term (Lever 1984). A typical material, K_3MnF_6, gives the following transition energies: $^5B_{1g}\rightarrow{}^5A_{1g}=1.12$ eV, $^6B_{1g}\rightarrow{}^5B_{2g}=2.16$, and $^5B_{1g}\rightarrow{}^5E_g=2.43$ eV (Allen and Warren 1971). The average value of the $^5B_{2g}$ and ^5E_g assignments gives 2.30 eV for the $(t_{2g})-b_{1g}$ separation. The close correspondence between the orbital splittings determined by optical spectroscopy for K_3MnF_6 and the EELS determined values for manganite lends further support to our orbital assignments for the Mn L_3-edge in manganosite.

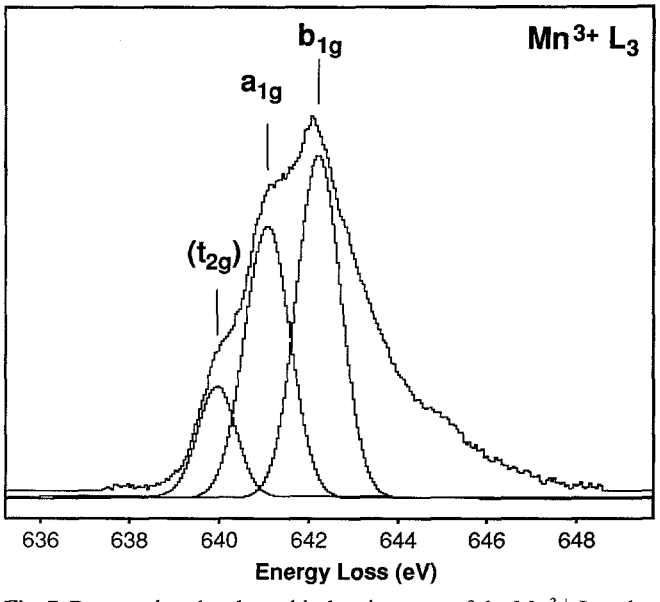

Fig. 7. Proposed molecular orbital assignment of the Mn^{3+} L_3-edge from manganosite assuming D_{4h} symmetry of the Mn. The three Gaussian peaks used to determine the positions of the partially resolved peaks are shown

It appears that the simple model splitting of the d-orbitals with D_{4h} symmetry explains some of the features on the Mn L_3-edge in manganite, gaudefroyite and norrishite. Although this simple MO approach appears to explain the Jahn-Teller distorted $^{[6]}Mn^{3+}$ L_3-edges, their similarity to the L_3-edge from bixbyite, which does not have similar sites to that in the other Mn^{3+} minerals studied, complicates the matter. This then leads to several possibilities. The MO description of the L_3-edge may be incorrect and the close correspondence between the MO states and the measurements on manganite is fortuitous. Alternatively, the MO may be correct and the combination of the two inequivalent sites in bixbyite may have produced a combined edge whose sum is an L_3-edge similar to manganite. This problem may be partly resolved by collecting the L_3-edge of Mn^{3+} in a regular or near regular octahedral environment as well as performing more detailed multiplet calculations for symmetries other than T_d and O_h.

Manganese IV

Octahedrally coordinated Mn^{4+} has the ground state configuration $^4A_{2g}$ $[(t^+{}_{2g})^3]$ in which there are no electrons in the e_g orbital. Several Mn^{4+} oxides were studied and they are all composed of various arrangements of manganese octahedra. The Mn $L_{2,3}$-edges are illustrated in Fig. 8 and have been arranged in order of decreasing energy between the two peaks on the L_3-edge, peaks (a) and (b). This energy difference varies from 2.6 eV in ramsdellite and pyrolusite to 2.1 eV in $SrMnO_3$.

$SrMnO_3$ forms an undistorted hexagonal (nonperovskite) polytype (Negas and Roth 1970; Battle et al. 1988) with six equivalent Mn–O bond lengths. All of the other Mn^{4+} oxides studied are natural oxides in which the $Mn-O_6$ octahedra join to form a variety of structures (Waychunas 1991). Asbolan and chalcophanite consist of a layer structure with sheets of edge-sharing MnO_6 octahedra. Todorokite is classified as a tunnel structure manganese oxide because trioctahedral slabs of MnO_6 octahedra share vertices which leave tunnels. Pyrolusite is composed of chains of edge-sharing MnO_6 octahedra whereas ramsdellite has double chains of edge-sharing MnO_6 octahedra. The MnO_6 octahedra in pyrolusite are nearly regular, slightly distorted in todorokite and more so in ramsdellite. Despite these distortions all of the Mn^{4+} materials studied give a double peaked L_3-edge with a maximum at ca. 644 eV and a weaker slightly asymmetrical L_2-edge.

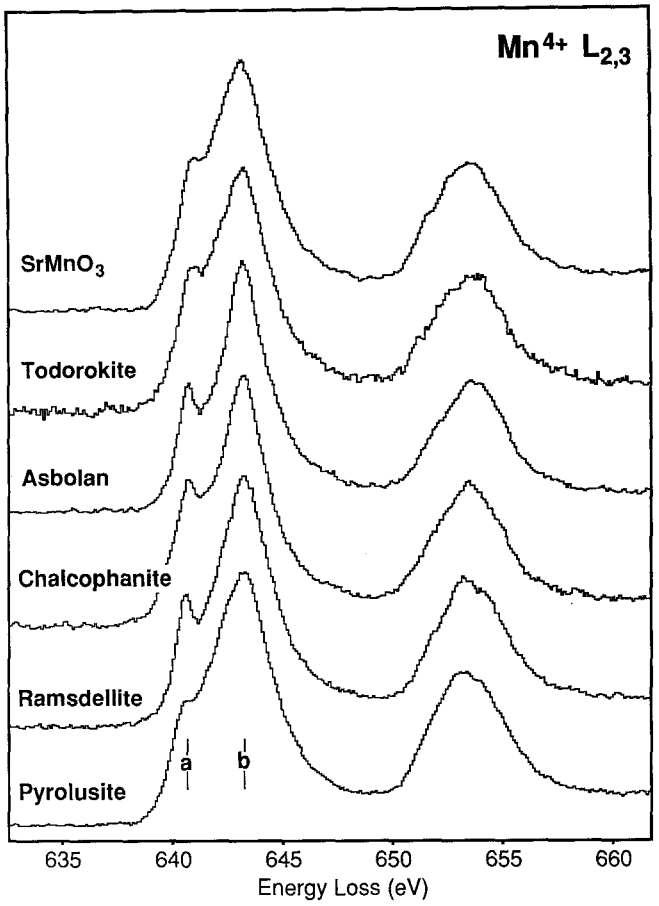

Fig. 8. Mn $L_{2,3}$-edges from the octahedrally coordinated Mn^{4+} containing materials ramsdellite, pyrolusite, chalcophanite, asbolan, todorokite and $SrMnO_3$. The spectra have been ordered from pyrolusite to asbolan with respect to decrease in the width at half height of the main L_3-edge, peak (b). Todorokite and $SrMnO_3$ are not included in this ordering as they contain, in addition to the dominant Mn^{4+}, some Mn^{3+}

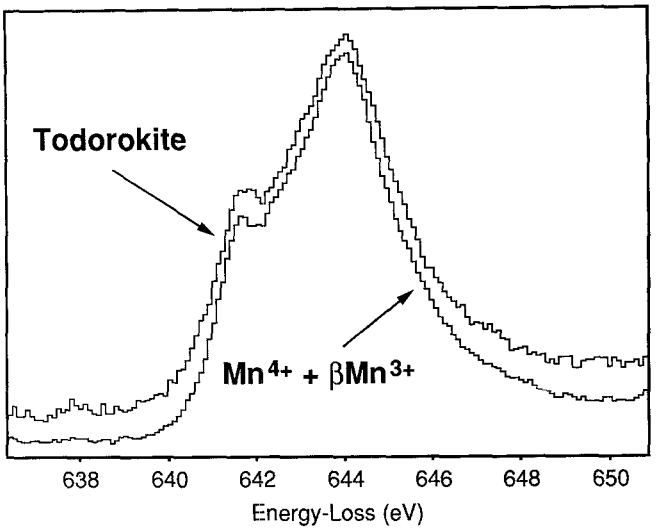

Fig. 9. The Mn L_3-edge from todorokite is simulated by adding a fraction β of the Mn L_3 spectrum from bixbyite to the L_3 spectrum from asbolan. (In principle the ratio Mn^{3+}/Mn^{4+} can be derived from β if a suitable calibration is performed.)

The energy difference between the two peaks on the L_3-edges in Fig. 8 are; pyrolusite (2.62 eV), ramsdellite (2.62 eV), chalcophanite (2.52 eV), asbolan (2.42 eV), todorokite (2.26 eV) and $SrMnO_3$ (2.12 eV). Neglecting the values from todorokite and $SrMnO_3$ for reasons that will be discussed shortly, the energy separation between the two L_3-edge peaks are similar in energy to 10Dq of 2.75 eV from K_2MnF_6 as determined by optical spectroscopy (Allen and Warren 1971). It is also similar to the energy splitting observed on their corresponding O K-edge pre-peak (see discussion) and the value of 3.3 eV determined by SCF Xα scattering method (Sherman 1984). Since all of the Mn^{4+} compounds studied here are octahedrally coordinated, without any large octahedral distortions, the d-orbitals are expected to be split into a lower energy t_{2g} and higher energy e_g orbital. Thus the two L_3 peaks, peaks (a) and (b), are initially identified as arising from transitions to orbitals with t_{2g} and e_g character, respectively.

The anomalously small 10Dq values measured from the L_3-edge of $SrMnO_3$ and todorokite may be caused by significant quantities of Mn^{3+} in the irradiated volume. While a quantitative determination of the mixed valences is beyond the scope of this paper (see Cressey et al. 1993 for an example of multivalent quantification using Fe $L_{2,3}$-edges), we do show that it is possible to simulate a mixed valent Mn $L_{2,3}$-edge by adding the appropriate amounts of the two single valent edges. It is possible to simulate the L_3-edge shapes from $SrMnO_3$ and todorokite by adding a suitable contribution of the L_3-edges from Mn^{3+} (bixbyite) to one of the Mn^{4+} edges. Figure 9 compares the L_3-edge from todorokite with a linear combination of the L_3-edges from asbolan (Mn^{4+}) and bixbyite (Mn^{3+}) showing that a similar edge shape is obtained when a suitable amount of Mn^{3+} is present in the sample. The effect of adding increasing amounts of Mn^{3+} to the Mn^{4+} L_3-edge is threefold: a) decrease in the energy separation between the two peaks on the L_3-edge, b) a corresponding increase in intensity in the region between the two L_3 peaks, and c) an increase in intensity of peak (a) relative to the intensity of the L_2 peak. In all of the pure Mn^{4+} compounds that do not contain any Mn^{3+} or Mn^{2+}, the t_{2g} peak on the L_3-edge is less intense than the L_2 peak. This strongly suggests that the L_3-edges from $SrMnO_3$ and todorokite contain some Mn^{3+} and illustrates the possibility of quantifying the oxidation states on a nanometer scale. The origin of the Mn^{3+} in the $SrMnO_3$ and todorokite is likely to be due to the electron beam reduction of the Mn^{4+} to Mn^{3+} (Garvie and Craven 1994a) as these materials were electron-beam sensitive. Another possibility for the presence of Mn^{3+} in todorokite is that it is present in the structure, substituting for Mn^{4+} to aid in charge compensation (Waychunas 1991).

The main L_3 peak from pyrolusite is apparently broader than those from ramsdellite, chalcophanite and asbolan. This is unlikely to be due to significant amounts of Mn^{3+} for the reasons listed above. Several samples of pyrolusite from a variety of sources have been studied (unpublished data) and they all resemble the pyrolusite

$L_{2,3}$-edge illustrated in Fig. 8. It is uncertain why pyrolusite has a different L_3 peak shape. However in their study of the Mn K-edge observed by XAS, Manceau et al. (1992) noted that the pre-peak intensities of a number of Mn^{4+} oxides were roughly proportional to the ratio of edge- to corner-sharing MnO_6 octahedra. Pyrolusite has the highest edge/corner ratio. Each octahedron shares six corners and two edges and gives the most intense K-edge pre-peak whereas the phyllomanganate buserite, which has a similar structure to asbolan, has no corner-sharing octahedra and the lowest pre-peak intensity. Mn^{4+} oxides with different ratios gave pre-peak intensities between the extremes of pyrolusite and buserite. Our EELS data also follows this ratio if we compare the widths at half height of the L_3 peak, which decreases in the order pyrolusite (3.8 eV), ramsdellite (3.2 eV), chalcophanite (2.8 eV) and asbolan (2.5 eV) with the edge/corner ratios for these minerals (Manceau and Combes 1988): pyrolusite (2/6), ramsdellite (4/4), chalcophanite (5/2) and asbolan (6/0). Thus the width of the main L_3-edge decreases with increase in the edge/corner ratio. The spectra for $SrMnO_3$ and todorokite are not included because as discussed above they may contain several percent of Mn^{3+} and so give anomalous L_3-edge widths.

Manganese VII

In the ionic picture of bonding, the Mn^{7+} compounds have empty d-orbitals and ground state character $^1A_1$ in both T_d and O_h symmetries. Most high-valent Mn compounds belong to the tetrahedrally bonded oxoanions MnO_4^{x-}, where x is 1 to 4. The only Mn^{7+} material investigated was potassium permanganate in which the d^0 manganese ion is tetrahedrally bonded to four oxygen anions (Palenik 1967). Figure 10 illustrates the $L_{2,3}$-edge for $KMnO_4$. The poor counting statistics on the Mn^{7+} $L_{2,3}$-edge are due to the short integration time used. This was necessary because of the extreme electron-beam sensitivity of the permanganate which was rapidly reduced to an edge which resembled $^{[6]}Mn^{4+}$ in both energy and shape. The L_2- and L_3-edges both show a single peak broadened on the low energy side and occurring at 645.6 eV and 656 eV respectively. Further evidence that this spectrum represents Mn^{7+} and not an intermediate valence is its similarity in shape to the Mn $L_{2,3}$-edge from potassium permanganate determined by XAS and several other d^0 transition element MO_4^{n-} oxo anions with M = Ti, V and Cr (Brydson et al. 1993) and to the Mn $L_{2,3}$-absorption edge in silver permanganate (unpublished data). The absence of pre-peaks to the L_3-edge, present in the other spectra in (Brydson et al. 1993) is probably due to the early stages of electron beam damage of the potassium permanganate.

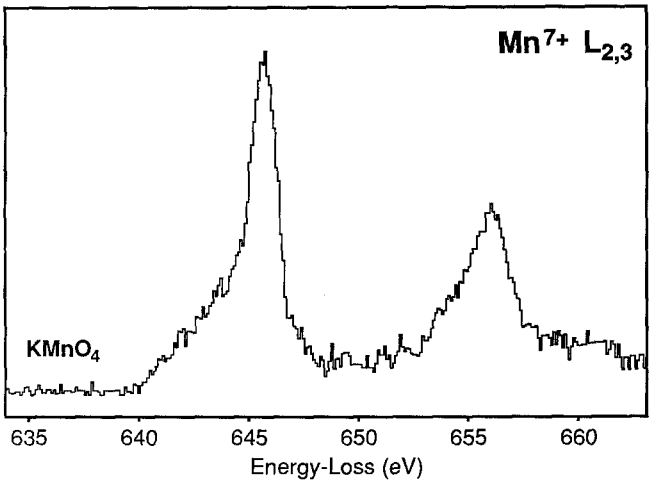

Fig. 10. Mn $L_{2,3}$-edge from potassium permanganate. The poor counting statistics of the edges are due to the extreme electron beam sensitivity of the material

Mixed Valence Oxides

Many mixed valence manganese materials exist and most commonly involve the valences II, III and IV. Several

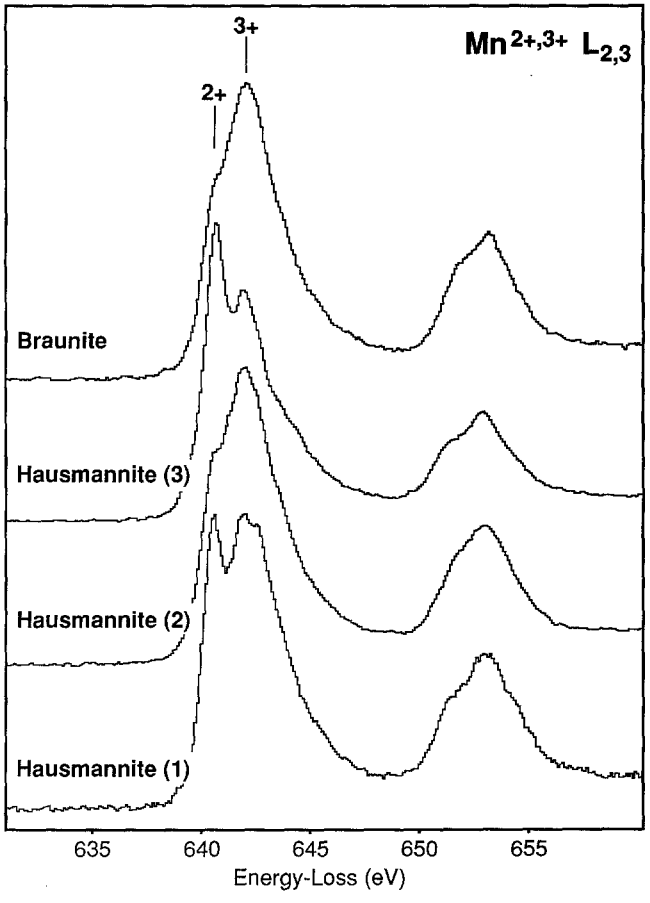

Fig. 11. Mn $L_{2,3}$-edges from the mixed Mn^{2+}, Mn^{3+} oxidation state minerals hausmannite and braunite. The *vertical bars* indicate the position of the Mn^{2+} and Mn^{3+} L_3 peak maxima. The Mn $L_{2,3}$-edge from hausmannite (1) is from a well crystallised mineral. Hausmannite (2) and (3) illustrate Mn $L_{2,3}$-edges from a sample of hausmannite that exhibited a range of $L_{2,3}$-edge shapes. The two spectra shown, hausmannite (2) and (3), represent the two extremes with a high-Mn^{3+} hausmannite(2), and high-Mn^{2+} hausmannite(3)

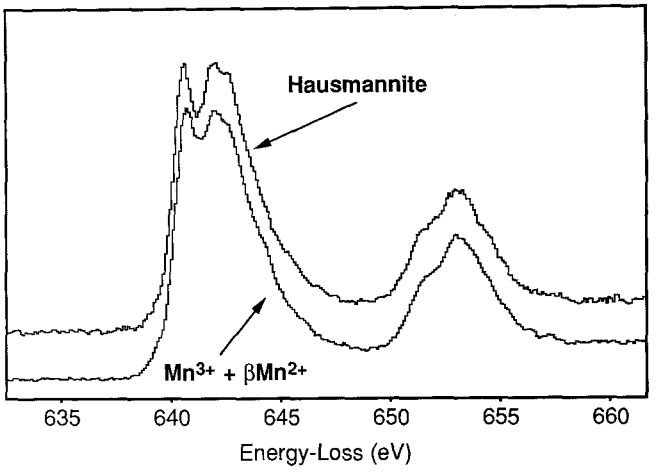

Fig. 12. The $L_{2,3}$-edges of hausmannite can be simulated by adding suitable proportions of $^{[4]}Mn^{2+}$ (jacobsite) and $^{[6]}Mn^{3+}$ (manganite)

well characterised mixed valence oxides are known such as α-Mn_3O_4 (II and III) and Mn_5O_8 (II and IV). Edges from two mixed valence minerals, hausmannite (α-$Mn^{2+}Mn^{3+}{}_2O_4$) and braunite ($Mn^{2+}Mn^{3+}{}_6SiO_{12}$), are illustrated in Fig. 11. Ideally, hausmannite is composed of $^{[4]}Mn^{2+}$ and $^{[6]}Mn^{3+}$ cations in the ratio 1:2. Since Mn^{3+} is subject to Jahn-Teller distortion this causes hausmannite to crystallise in a tetragonally distorted spinel structure (Kaczmarek and Wolska 1993). The L_3-edge for hausmannite(1) consists of an initial sharp peak at 640.2 eV characteristic of Mn^{2+} followed by a double-peaked maximum at 641.8 eV indicative of Mn^{3+}. The lack of a separate low-energy peak on the Mn^{2+} L_3-edge suggests that the Mn does not occupy a regular octahedral environment although, as shown above, it is not possible to be more specific about the symmetry of the Mn^{2+} environment. The $L_{2,3}$-edge from hausmannite can be simulated by a suitable linear combination of $^{[4]}Mn^{2+}$ (jacobsite) and $^{[6]}Mn^{3+}$ (manganite). This is illustrated in Fig. 12 which compares the $L_{2,3}$-edges from hausmannite(1) with a simulated profile. All of the features of the experimental $L_{2,3}$-edge are faithfully reproduced in the simulated edge including the double peaked Mn^{3+} L_3 peak.

Braunite contains four distinct Mn sites with various Mn–O distances (Moore and Araki 1976); these sites are $^{[8]}Mn^{2+}$ and three different $^{[6]}Mn^{3+}$. The braunite $L_{2,3}$-edge has a peak maximum at ca. 642 eV consistent with dominant Mn^{3+} and the presence of Mn^{2+} is visible on the low energy side of the L_3-edge. The overall L_3-edge shape is similar to that of manganite, the main difference being the stronger pre-peak due to Mn^{2+}. The L_3 peak maximum does not have the same shape as that of bixbyite or the single site Jahn-Teller distorted minerals and is expected to reflect the three different $^{[6]}Mn^{3+}$ sites.

Two further $L_{2,3}$-edges are illustrated in Fig. 11 labelled hausmannite(2) and (3). These spectra are from a different sample of hausmannite that exhibited a variety of different Mn $L_{2,3}$-edge shapes characteristic of large variations in the Mn^{3+}/Mn^{2+} ratio. The spectra illustrated represent the two extremes while many of the spectra had the same shape as the well crystallised hausmannite(1). Hausmannite(2) has an $L_{2,3}$-edge with the same shape and energy as that from braunite whereas hausmannite(3) contains predominantly Mn^{2+}.

Discussion

Edge Energies, Chemical Shifts and Crystal-Field Strengths

For any single oxidation state the relative peak positions were found to be very similar. Energies for the various Mn compounds are very close to their corresponding oxides and no discrepancies were noticed among the high-spin compounds. Table 3 compares the energy values of the Mn L_3-edge from several Mn compounds with data obtained from Rask et al. (1987) and Paterson and Krivanek (1990). The absolute energy values obtained by Rask et al. are different from those presented in this work although the relative peak positions are in good agreement even though their spectra were collected with an energy resolution of ca. 1 eV. In general

Table 3. Absolute energy of the L_3-edge for MnO from this work and relative L_3-edge values for five Mn materials. The energy difference relative to MnO are given for each sample. The data for this work are compared with values obtained from Rask et al. (1987) and Paterson and Krivanek (1990). Error for MnO L_3-edge is ± 0.5 eV. Error for the other materials is ± 0.2 eV

Material	This work	s.w.r.t[a] MnO	Rask et al. (1987)[b]	s.w.r.t MnO	Paterson & Krivanek (1990)	s.w.r.t MnO
Mn	641.3	−1.0	641.3	−1.1	–	–
MnO	640.3	0	640.2	0	639.0	0
Mn_2O_3	641.8	+1.5	641.6	+1.4	639.6	+0.6
γ-MnOOH	642.5	+2.2	642.4	+2.2	–	–
β-MnO_2	643.8	+3.5	644.3	+4.1	642.1	+3.1
$KMnO_4$	645.6	+5.3	–	–	–	–
Error	± 0.2 (± 0.5 eV)		± 0.2–± 0.67		± 0.4	

[a] s.w.r.t-shift with respect to

[b] To aid comparison with data in the present work the Mn value from Rask et al. (1987) was made equal to our Mn value and the difference (Rasks value 2.3 eV higher) subtracted

the Mn L_3-edges systematically shift to higher energy with increase in the formal valence of the Mn ion from a minimum of ca. 639.5 eV in α-$Mn^{2+}S$, 642.5 eV in γ-$Mn^{3+}OOH$, 643.8 eV in β-$Mn^{4+}O_2$ to 645.6 eV in $KMn^{7+}O_4$. The only material studied which did not follow this sequence was metallic manganese which has a peak maximum at a higher energy than the Mn^{2+} compounds.

The strength of the crystal-field and hence the crystal-field splitting, as measured on the L_3-edges, increased with increase in the formal oxidation state of the manganese. This is due to two effects: a larger electrostatic interaction between the Mn cations and O anions; and an increased degree of e_g σ-relative to t_{2g} π-bonding in the MnO_6 octahedron. The latter effect is caused by a decrease in the Mn–O bond lengths with increase in oxidation state: typical average Mn–O distances are manganosite (2.22 Å), manganite (2.10 Å), and pyrolusite (1.89 Å). The 10Dq values measured for manganosite, manganite and pyrolusite from the experimental Mn L_3-edges were 1.13 eV, 2.3 eV, to 2.6 eV, respectively.

Comparison with Theoretical $L_{2,3}$ Spectra

Figure 13 compares the experimental $L_{2,3}$-edges from manganosite, manganite and ramsdellite with selected calculated 2p atomic multiplet spectra of van der Laan and Kirkman (G. van der Laan, private communication). The spectra were calculated using the ligand-field multiplet approach (van der Laan and Kirkman 1992) with O_h symmetry and take into account the following interactions in calculating the dipole transitions from $2p^63d^n$ to $2p^53d^{n+1}$: 2p–3d and 3p–3p Coulomb and exchange interactions; 2p and 3p spin-orbit interactions; and the crystal-field interaction. Effects such as hybridisation were not included in the calculations so bonding of 3d TM with strongly electronegative anions, where the bonding is dominantly ionic, should give calculated spectra that are closely related to experimental edges. Bonding in ionic compounds can be described in terms of an integer number of electrons being transferred from cation to anion sites. It is then possible to describe the 3d transition metal edges by a $3d^n \rightarrow 2p^53d^{n+1}$ transition. When a significant amount of covalency is present, either due to less electronegative anions or higher formal valency on the 3d transition metal, the d-count can be thought of as having a non-integer number. As the covalency increases the bonding between the metal and the ligand can be described less and less as a $3d^n \rightarrow 2p^53d^{n+1}$ transition with a single initial ground state configuration. Instead, two or more ground state electronic configurations are present in the initial state multiplet and so the atomic multiplet spectrum will reflect the different ground states thus giving an averaged edge. Thole et al. (1985) has calculated the Mn d^5 2p atomic multiplet spectra for various possible ground state terms. The resulting spectra exhibit very different $L_{2,3}$-edge shapes, and so demonstrate the high sensitivity of the $L_{2,3}$-edge shapes to the ground state electronic configuration and term. For compounds in which covalency is important, the ground state of the 3d TM can be described as a combination of $3d^n$ and $3d^{n+1}L$, where L denotes a ligand hole. Thus significant amounts of hybridisation between the ligand p and transition metal 3d orbitals can result in changes in the multiplet structures and the appearance of satellite structures (Thole et al. 1985; van der Laan et al. 1986, 1992).

The Mn^{2+} $L_{2,3}$-edge from manganosite was successfully modelled by the atomic multiplet spectrum with O_h symmetry and crystal-field strength of 1.0 eV (Fig. 13a). All of the features on the experimental edge are reproduced in the theoretical edge and illustrate that the threshold features of the $L_{2,3}$-edge are due to multiplet structure. The experimental $^{[6]}Mn^{3+}$ L_3-edge in Fig. 13b is quite dissimilar to the L_3-edge calculated for Mn d^4 in O_h symmetry with a crystal-field strength of 2.5 eV. The L_3-edges for the Mn^{4+} minerals studied are similar in shape to the calculated L_3-edge for Mn^{4+} with O_h symmetry and a 10Dq of 2.5 eV (Fig. 13c). The calculated and experimental L_3-edges differ in the shape of the e_g peak which is split into two peaks in the calculated multiplet spectra. There is no sign in any of the

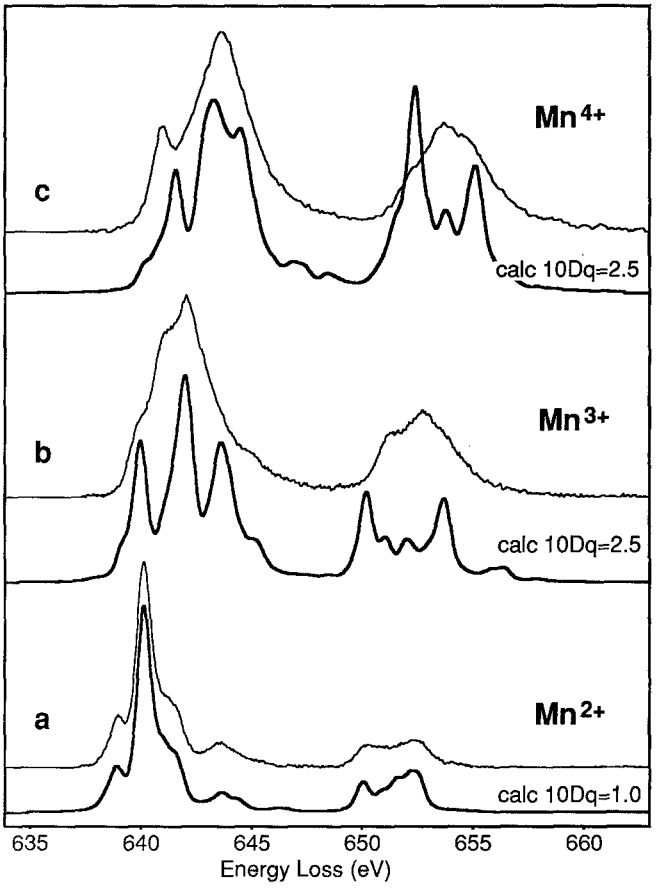

Fig. 13a–c. Comparison of theoretical (*thick line*) and experimental (*thin line*) multiplet L_3-edges. The theoretical 2p atomic multiplet spectra were calculated by van der Laan and Kirkman (1992) in O_h symmetry. The strength of the crystal-field, 10Dq, is listed for each spectrum. **a** L_3-edge from manganosite compared with the theoretical edge with a cubic crystal field strength of 1.0 eV. **b** L_3-edge from manganite and theoretical L_3-edge with a cubic crystal field of 2.5 eV. **c** The L_3-edge from ramsdellite and theoretical L_3-edge with a cubic crystal field of 2.5 eV

experimental $^{[6]}Mn^{4+}$ L_3-edges of the main L_3-edge being split.

The close similarity between the experimental and theoretical L_3-edge for Mn^{2+} can be attributed to the low covalent nature of the Mn–O bond in manganosite. The differences between the $^{[6]}Mn^{3+}$ and $^{[6]}Mn^{4+}$ L_3-edges in comparison to the theoretical L_3-edges calculated for O_h symmetry may be due to two main reasons-covalency and site symmetry effects. Sherman (1984) has shown that the covalency of the Mn–O bond increases markedly from 29% in Mn^{2+}–O, 69% in Mn^{3+}–O, to 73% in Mn^{4+}–O. This high degree of covalency may then explain the dissimilar experimental and calculated Mn^{3+} and Mn^{4+} L_3-edges. Covalency effects have been observed in NiO and NiX where X is an F, Cl, Br or I (van der Laan et al. 1986) and Cu minerals (van der Laan et al. 1992). The nickel compounds bonded to highly electronegative anions gave 2p XAS spectra which could be matched against the calculated 2p absorption edges in which the transition could be described as $3d^n \rightarrow 2p^5 3d^{n+1}$. With a decrease in electronegativity and an associated increase in covalent bonding, satellite spectra appeared which were not present in NiO and NiF_2. Evidence for covalency effects is given in the next section. For the Mn^{3+} compounds there is the added problem in that the calculated edge shown in Fig. 13b has been calculated for O_h symmetry, and as described above, d^4 compounds are Jahn-Teller unstable and exhibit tetragonal distortion. This is likely to introduce new multiplet structure into the edge which is forbidden in O_h symmetry. It is uncertain why the experimental L_2-edges for Mn^{3+} and Mn^{4+} are so dissimilar to the theoretical multiplet L_2-edges whereas the Mn^{2+} L_2-edges are very similar.

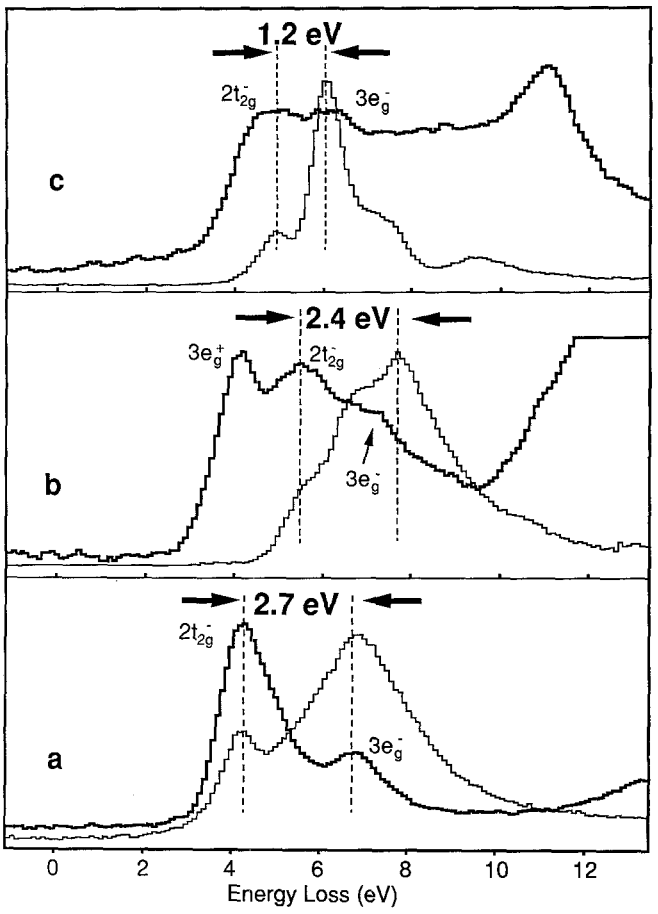

Fig. 14a–c. Comparison of the O K-edge pre-peak (*bold*) and Mn L_3-edge from **a** manganosite, **b** manganite and **c** ramsdellite. The *dashed vertical lines* define 10Dq from the Mn L_3-edges as described in the text. The Mn L_3-edges are then aligned with the corresponding molecular orbital peaks on the oxygen K-edge pre-peak. The O K-edges have been assigned MOs according to the text

Comparison of the O K-Edge with the Mn L_3-Edge

Several EELS and XAS studies have described the O K ELNES of the 3d TM (de Groot et al. 1989; Paterson and Krivanek 1990; Krivanek and Paterson 1990; Kurata and Colliex 1993; Kurata et al. 1993). The O K-edge can be divided into two distinct regions (de Groot et al. 1989), a pre-peak region which results from O 2p weight in predominantly 3d character, and a broader region extending some 50 eV beyond the pre-peak region which is attributed to O p weight hybridised with metal 4s and 4p states. The pre-peak region can be described in terms of a model incorporating ligand-field splitting and exchange splitting (Kurata and Colliex 1993). The O K-edge pre-peak region of the 3d-transition metal oxides is often split into two peaks, with the energy difference between these peaks being almost identical to the ligand-field splitting determined by optical spectroscopy (de Groot et al. 1989). As the O K-edge pre-peak appears to reflect the strength of 10Dq this then gives us the opportunity to compare the 10Dq determined from the Mn L_3-edges with the value obtained from the corresponding O K-edge. This comparison is readily achieved with the Mn^{4+} L_3- and O K-edges because the O K-edge pre-peak shows a double peaked structure of which the two peaks can be assigned to the 2_{t2g}^- and $3e_g^-$ molecular orbitals (Kurata and Colliex 1993). This is illustrated in Fig. 14a which compares the O K-edge pre-peak and Mn L_3-edge for ramsdellite (MnO_2). The pre-peak of the Mn L_3-edge, which we have attributed to transitions to states of t_{2g} character, is aligned with the first O K-edge pre-peak. The broadening on the high-energy side of the $2t_{2g}^-$ peak of the O K-edge can be assigned to the unresolved $3e_g^+$ MO which is separated by ca. 0.3 eV from the $2t_{2g}^-$ peak as calculated using the spin unrestricted self-consistent field SCF Xα calculation of the MOs in the MnO_6^{10-} cluster (Sherman 1984). The energy difference between $2t_{2g}^-$ and $3e_g^-$ orbitals measured from the O K-edge in ramsdellite is 2.52 eV which is very close to the value of 2.62 eV measured on the Mn L_3-edge.

A similar comparison can be made for the Mn^{3+} L_3 and O K-edges for manganite (Fig. 14b) although the interpretation is not quite as simple. This is because the O K-edge pre-peak consists of two distinct peaks followed by a peak of lower intensity. The three peaks on the O K-edge pre-peak for Mn^{3+} have been assigned to transitions to the $3e_g^+$, $2t_{2g}^-$ and $3e_g^-$ unoccupied states

(Kurata and Colliex 1993). The first partially resolved peak on the Mn L_3-edge, which we earlier assigned to a peak due to transitions of b_{2g}/e_g character, has been aligned with the $2t_{2g}^-$ peak for the O K-edge. It is then possible to see from Fig. 14b that the peak maximum of the Mn L_3-edge corresponds with the weak peak labelled $3e_g^-$ on the O K-edge. The energy separation between $2t_{2g}^-$ and $3e_g^-$ on the O K-edge, and hence the value of the ligand-field splitting is close to the 10Dq of 2.3 eV measured on the Mn L_3-edge in manganite. In an earlier section the manganite L_3-edge was described in terms of a weak field tetragonal splitting of the d orbitals. This would also imply that the orbital assignments of the O K-edge should reflect this symmetry. The fairly sharp $2t_{2g}^-$ peak on the O K-edge is not split into two peaks consistent with the expected weak splitting of the t_{2g} orbital in D_{4h} symmetry. The peak maximum of the Mn L_3-edge aligns well with the "$3e_g^-$" peak on the O K-edge but in D_{4h} symmetry the e_g orbital should split into two orbitals a_{1g} and b_{1g}. The a_{1g} orbital is only partially resolved on the Mn L_3-edge and if present on the O K-edge, it would be difficult to detect on the slope between the peaks labelled $2t_{2g}^-$ and $3e_g^-$. Despite these difficulties, the value of 10Dq measured for manganite on the O K-edge pre-peak is almost the same as that measured on the L_3-edge.

In Fig. 14c, the Mn L_3- and O K-edges from manganosite are compared. The two O K-edge pre-peaks have been identified as arising from transitions to accessible unoccupied final states of $2t_{2g}^-$ and $3e_g^-$ character (Kurata and Colliex 1993). The peak splitting of ca. 1.1 eV between the first two peaks on the Mn L_3-edge is possibly reproduced on the O K-edge pre-peak although is difficult to be certain of this because of the broad weak features on the O K-edge in manganosite.

Conclusions

The high-resolution PEELS spectra from the Mn $L_{2,3}$ materials illustrate a great variety of multiplet structures. The experimental set-up allows data to be collected with a resolution of ca. 0.5 eV at the Mn L_3-edge which is comparable to that obtained from medium to high-resolution XANES with a synchrotron source. PEELS performed in a STEM has the added advantage, over XAS, of high spatial resolution, down to 2.2 Å (Browning et al. 1993), which would be ideal for studying low-dimensionality systems such as mineral interfaces and exsolution lamellae.

Consistent with previous EELS work on Mn containing mineral, the Mn $L_{2,3}$-edges show large variations in their edge shapes with change in oxidation state of the manganese. These changes can be used as a valence fingerprint. The Mn $L_{2,3}$-edges from Mn^{2+} were not found to be sensitive to the local site symmetry of the ligands. This implies that the Mn^{2+} $L_{2,3}$-edges are not very useful for detecting small changes in the transition-metal site symmetry although a nearly regular octahedral environment will be manifested by a pre-peak on the Mn L_3-edge. For octahedrally coordinated Mn^{2+}, the lack of the pre-peak appears to be related to a highly distorted octahedron, as illustrated by the Mn L_3-edge from lithiophorite. A tentative fingerprint for the Jahn-Teller distorted environment was recognised for the Mn^{3+} cation in minerals.

We have shown that it is possible to determine the crystal-field strength from the Mn L_3-edges. This was substantiated by comparing the 10Dq measured from the Mn L_3-edges with published results determined by optical spectroscopy for similar compounds and also by showing that the same splitting is observed on the O K-edge pre-peaks of the oxides. Optical spectroscopic techniques have been used extensively to determine 10Dq from Mn^{2+} and to a lesser extent minerals containing small amounts of Mn^{3+}. It is exceedingly difficult to determine 10Dq for Mn^{3+} and Mn^{4+} oxides by transmission optical means because very thin samples are needed to allow adequate light transmission. The ease with which 10Dq can be determined from the Mn^{3+} and Mn^{4+} $L_{2,3}$- and O K-edges will undoubtedly make EELS an important technique for crystal-field strength determinations.

The close correspondence between the theoretical and experimental Mn^{2+} L_3-edge from manganosite can be explained by its highly ionic nature and the fact that the Mn sits in a nearly regular octahedral site. Both the Mn^{3+} and Mn^{4+} L_3-edges show significant differences in comparison to the theoretical 2p multiplet spectra. This can be explained in part by the highly covalent nature of the Mn–O bonds in manganite and ramsdellite and it is expected that the $L_{2,3}$-edges will be strongly modified by the molecular orbital nature of the metal to ligand bonds. An additional factor for the Mn^{3+} compounds is the distortion of the octahedron due to the Jahn-Teller effect which will further modify the atomic multiplet spectrum. In order to identify the components in the Mn^{3+} $L_{2,3}$-edges that belong to the covalency and the tetragonal distortion, further theoretical 2p atomic multiplet spectra will need to be calculated for Mn d^4 for symmetries other than O_h and T_d.

Acknowledgements. We would like to thank the following for kindly donating samples for our research: Prof. G.C. Allen (Interface Analysis Centre, University of Bristol) for the synthetic jacobsite; Dr. J. Faithfull (Huntarian Museum, Glasgow) for the samples of alabandite (M9916), hausmannite (M8097), manganite (M6481), rhodochrosite (Rotley 1425), rhodonite (M6728), and spessartine (M7135); Prof. S. Guggenheim (University of Illinois at Chicago, USA) for the sample of norrishite; and Dr. H. Miura (Dept. Geology and Mineralogy, Faculty of Science, Hokkaido University, Japan) for the sample of ramsdellite. We are also grateful to Dr. G. van der Laan (SERC Daresbury Laboratory) for providing the theoretical Mn $L_{2,3}$ multiplet spectra. The authors would like to thank the Science and Engineering Research Council for providing funds to purchase the Gatan 666 parallel electron energy loss spectrometer and for a post-doctoral research assistantship for one of us (LG). Finally we are grateful to Dr. R. Brydson for his many helpful discussions during the preparation of this manuscript.

References

Abbate M, de Groot FMF, Fuggle JC, Fujimori A, Tokura Y, Fujishima Y, Strebel O, Domke M, Kaindl G, van Elp J, Thole

BT, Sawatzky GA, Sacchi M, Tsuda N (1991) Soft-x-ray-absorption studies of the location of extra charges induced by substitution in controlled-valence materials. Phys Rev B 44:5419–5422

Allen GC, Warren KD (1971) The electronic spectra of the hexafluoro complexes of the first transition series. Struct Bonding 9:49–138

Allan GC, Jutson JA, Tempest PA (1988) Characterisation of manganese-chromium-iron spinel-type oxides. J Nucl Mater 160:34–47

Battle PD, Gibb TC, Jones CW (1988) The structural and magnetic properties of $SrMnO_3$: a reinvestigation. J Solid State Chem 74:60–66

Belov VF, Pyl'nev VG, Zheludev IS, Korovushkin VV, Korneev EV, Yarmukhamedov YuN (1975) Study of ferroelectric boracite $Mn_3B_7O_{13}Cl$ by the nuclear gamma resonance method. Sov Phys Crystallogr 20:96–97

Browning ND, Chisholm MF, Pennycook SJ (1993) Atomic-resolution chemical analysis using a scanning transmission electron microscope. Nature 366:143–146

Brydson R (1991) Interpretation of near-edge structure in the electron energy-loss spectrum. Bull Electron Micro Soc Am 21:55–64

Brydson R, Sauer H, Engel W (1992) Electron energy loss near-edge structure as an analytical tool- the study of minerals. In: Disko MM, Ahn CC, Fultz B (eds) Transmission Electron Energy Loss Spectrometry in Materials Science. The Minerals, Metals & Materials Society, Warrendale, pp 131–154

Brydson R, Garvie LAJ, Craven AJ, Sauer H, Hofer F, Cressey G (1993) $L_{2,3}$-edges of tetrahedrally coordinated d^0 transition metal oxoanions XO_4^{n-}. J Phys Cond Matter 5:9379–9392

Cotton FA, Wilkinson G (1988) Advanced inorganic chemistry (Fifth Edition). John Wiley & Sons, New York

Cramer SP, de Groot FMF, Ma Y, Chen CT, Sette F, Kipke CA, Eichhorn DM, Chan MK, Armstrong WH, Libby E, Christou G, Brooker S, McKee V, Mullins OC, Fuggle JC (1991) Ligand field strengths and oxidation states from manganese L-edge spectroscopy. J Am Chem Soc 113:7937–7940

Cressey G, Henderson CMB, van der Laan B (1993) Use of L-edge x-ray absorption spectroscopy to characterise multiple valence states of 3d transition metals; a new probe for mineralogical and geochemical research. Phys Chem Minerals 20:111–119

de Groot FMF, Grioni M, Fuggle JC, Ghijsen J, Sawatzky GA, Petersen H (1989) Oxygen 1s x-ray-absorption edges of transition-metal oxides. Phys Rev B 40:5715–5723

de Groot FMF, Fuggle JC, Thole BT, Sawatzky GA (1990a) $L_{2,3}$ x-ray absorption edges of d^0 compounds: K^+, Ca^{2+}, Sc^{3+}, and Ti^{4+} in O_h (octahedral) symmetry. Phys Rev B 41:928–937

de Groot FMF, Fuggle JC, Thole BT, Sawatzky GA (1990b) 2p x-ray absorption of 3d transition-metal compounds: an atomic multiplet description including the crystal-field. Phys Rev B 42:5459–5468

de Groot FMF, Figueiredo MO, Basto MJ, Abbate M, Petersen H, Fuggle JC (1992) 2p x-ray absorption of titanium in minerals. Phys Chem Minerals 19:140–147

de Groot FMF, Abbate M, van Elp J, Sawatzky GA, Ma YJ, Chen CT, Sette F (1993) Oxygen 1s and cobalt 2p x-ray absorption of cobalt oxides. J Phys Cond Matter 5:2277–2288

Dowty E, Clark JR (1973) Crystal-structure refinements for orthorhombic boracite, $Mg_3ClB_7O_{13}$, and trigonal, iron-rich analogue. Z Kristallogr 138:64–99

Duffy JA (1990) Bonding, energy levels and bands in inorganic solids. Longman Scientific & Technical, Harlow

Egerton RF (1986) Electron energy-loss spectroscopy in the electron microscope. Plenum Press, New York

Fink J (1985) Electron energy-loss spectroscopy applied to solids. Z Phys B: Cond Matter 61:463–468

Fink J, Müller-Heinzerling Th, Scheerer B, Speier W, Hillebrecht FU, Fuggle JC, Zaanen J, Sawatzky GA (1985) 2p absorption spectra of the 3d elements. Phys Rev B 32:4899–4904

Furuseth S, Kjekshus A (1965) On the properties of α-MnS and MnS_2. Acta Chem Scand 19:1405–1410

Garvie LAJ, Craven AJ (1993) Determination of the crystal-field strength in manganese compounds by parallel electron energy loss spectroscopy. In: Craven AJ (ed) Proceedings of the Institute of Physics Electron Microscopy and Analysis Group. Institute of Physics Conference Series vol. 138, Bristol, pp 31–34

Garvie LAJ, Craven AJ (1994a) Electron beam induced reduction of Mn^{4+} in manganese oxides as revealed by parallel EELS. Ultramicroscopy (in press)

Garvie LAJ, Craven AJ (1994b) Use of electron-loss near-edge fine structure in the study of minerals. Am Mineral (in press)

Geller S (1971) Structures of α-Mn_2O_3, $(Mn_{0.983}Fe_{0.017})_2O_3$ and $(Mn_{0.37}Fe_{0.63})_2O_3$ and relation to magnetic ordering. Acta Cryst B 27:821–828

Geller S, Durand JL (1960) Refinement of the structure of LiMnPO$_4$. Acta Cryst 13:325–331

Holloway WM Jr, Giordano TJ, Peacor DR (1972) Refinement of the crystal structure of helvite, $Mn_4(BeSiO_4)_3S$. Acta Cryst B 28:114–117

Kaczmarek J, Wolska E (1993) Cation and vacancy distribution in nonstoichiometric hausmanite. J Solid State Chem 103:387–393

Keester KL, White WB (1968) Crystal-field spectra and chemical bonding in manganese minerals. The Mineralogical Society, International Mineralogical Association, London, pp 22–35

Köhler P, Massa W, Reinen D, Hofmann B, Hoppe R (1978) Der Jahn-Teller Effect des Mn^{3+}-Ions in oktaedrischer Fluokoordination. Ligandenfeldspektroskopische und magnetische Untersuchungen. Z Anorg Allg Chem 446:131–158

Krishnan KM (1990) Iron $L_{3,2}$ near-edge fine structure studies. Ultramicroscopy 32:309–311

Krivanek OL, Paterson JH (1990) ELNES of 3d transition-metal oxides I. Variations across the periodic table. Ultramicroscopy 32:313–318

Krivanek OL, Ahn CC, Keeney RB (1987) Parallel detection electron spectrometer using quadrupole lenses. Ultramicroscopy 22:103–116

Kurata H, Colliex C (1993) Electron energy-loss core edge structures in manganese oxides. Phys Rev B (in press)

Kurata H, Nagai K, Isoda S, Kobayashi T (1990) ELNES of iron compounds. In: Peachey LD, Williams DB (eds) Proceedings of the XIIth International Congress for Electron Microscopy, Volume 2: Analytical Sciences. San Francisco Press, San Francisco, pp 28–29

Kurata H, Colliex C, Brydson R (1993) ELNES structures in the oxygen K-edge spectra of transition metal oxides. Phys Rev B 47:13763–13768

van der Laan G, Kirkman IW (1992) The 2p absorption spectra of 3d transition metal compounds in tetrahedral and octahedral symmetry. J Phys Cond Matter 4:4189–4204

van der Laan G, Zaanen J, Sawatzky GA, Karnatak R, Esteva JM (1986) Comparison of x-ray absorption with x-ray photoemission of nickel dihalides and NiO. Phys Rev B 33:4253–4263

van der Laan G, Thole BT, Sawatzky GA, Verdaguer M (1988) Multiplet structure in the $L_{2,3}$ x-ray absorption spectra: a fingerprint for high- and low-spin Ni^{2+} compounds. Phys Rev B 37:6587–6589

van der Laan G, Pattrick RAD, Henderson CMB, Vaughan DJ (1992) Oxidation state variations in copper minerals studied with Cu 2p X-ray absorption spectroscopy. J Phys Chem Sol 53:1185–1190

Leapman RD, Grunes LA, Fejes PL (1982) Study of the $L_{2,3}$ edges in the 3d transition metals and their oxides by electron-energy-loss spectroscopy with comparisons to theory. Phys Rev B 26:614–635

Lever ABP (1984) Inorganic Electronic Spectroscopy (2nd Edition). Elsevier, Amsterdam, Holland

Manceau A, Combes JM (1988) Structure of Mn and Fe oxides and oxyhydroxides: a topological approach. Phys Chem Miner 15:283–295

Manceau A, Llorca S, Calas G (1987) Crystal chemistry of cobalt and nickel in lithiophorite and asbolane from New Caledonia. Geochim Cosmochim Acta 51:105–113

Manceau A, Gorshkov AI, Drits VA (1992) Structural chemistry of Mn, Fe, Co and Ni in manganese hydrous oxides: Part I. Information from XANES spectroscopy. Am Mineral 77:1133–1143

Manning PG (1967) The optical absorption spectra of garnets almandine-pyrope, pyrope and spessartine and some structural interpretations of mineralogical significance. Canad Mineral 9:237–251

Mattheiss LF, Dietz RE (1980) Relativistic tight-binding calculation of core-valence transitions in Pt and Au. Phys Rev B 22:1663–1676

Miura H, Kudou H, Ho Choi J, Hariya Y (1990) The crystal structure of ramsdellite from Pirika Mine. J Fac Sci, Hokkaido Univ, Ser IV, 22:611–617

Moore PB, Araki T (1976) Braunite: its structure and relationship to bixbyite, and some insights on the genealogy of fluorite derivative structures. Am Mineral 61:1226–1240

Negas T, Roth RS (1970) The system $SrMnO_{3-x}$. J Solid State Chem 1:409–418

Oelkrug D (1971) Absorption spectra and ligand field parameters of tetragonal 3d-transition metal fluorides. Struct Bonding 9:1–26

Otten MT, Buseck PR (1987) The oxidation state of Ti in hornblende and biotite determined by electron energy-loss spectroscopy, with inferences regarding the Ti substitution. Phys Chem Minerals 14:45–51

Palenik GJ (1967) Crystal structure of potassium permanganate. Inorg Chem 6:503–507

Paterson JH, Krivanek OL (1990) ELNES of 3d transition-metal oxides II. Variations with oxidation state and crystal structure. Ultramicroscopy 32:319–325

Pratt GW Jr, Coelho R (1959) Optical absorption of CoO and MnO above and below the Néel temperature. Phys Rev 116:281–286

Rask JH, Miner BA, Buseck PR (1987) Determination of manganese oxidation states in solids by electron energy-loss spectroscopy. Ultramicroscopy 21:321–326

Sherman DM (1984) The electronic structure of manganese oxide minerals. Am Mineral 69:788–799

Smyth JR, Bish DL (1988) Crystal structures and cation sites of the rock-forming minerals. Allen & Unwin, Boston, USA

Stout JW (1959) Absorption spectrum of manganous fluoride. J Chem Phys 31:709–719

Thole BR, Cowan RD, Sawatzky GA, Fink J, Fuggle JC (1985) New probe for the ground-state electronic structure of narrow-band and impurity systems. Phys Rev B 31:6856–6858

Tyrna PL, Guggenheim S (1991) The crystal structure of norrishite: $KLiMn_2^{3+}Si_4O_{12}$. Am Mineral 76:266–271

Waddington WG, Rez P, Grant IP, Humphreys CJ (1986) White lines in the $L_{2,3}$ electron-energy-loss and x-ray absorption spectra of 3d transition metals. Phys Rev B 34:1467–1473

Waychunas GA (1991) Crystal chemistry of oxides and oxyhydroxides. In: Lindsley DH (ed) Spectroscopic methods in mineralogy and geology. Mineralogical Society of America, Reviews in Mineralogy vol 25, pp 11–68

Yakubovich OV, Simonov MA, Belov NV (1975) Structure refinement for gaudefroyite. Sov Phys Crystallogr 20:87–88

Yamaguchi T, Shibuya S, Suga S, Shin S (1982) Inner-core excitation spectra of transition metal compounds: II. p–d absorption spectra. J Phys C Solid State 15:2641–2650